Inorganic Chemistry

Article

pubs.acs.org/IC

Two Metal–Organic Frameworks Constructed from One-Dimensional Cobalt(II) Ferrimagnetic Chains with Alternating Antiferromagnetic/Ferromagnetic and AF/AF/FM Interaction: Synthesis, Structures, and Magnetic Properties

Fen Yang, Baiyan Li, Wei Xu, Guanghua Li, Qi Zhou, Jia Hua, Zhan Shi,* and Shouhua Feng

State Key Laboratory of Inorganic Synthesis & Preparative Chemistry, College of Chemistry, Jilin University, Changchun 130012, P. R. China

Supporting Information

ABSTRACT: Here, we report two three-dimensional metal–organic frameworks of formula $[Co_2(4\text{-ptz})_2(bpp)(N_3)_2]_n$ (**1**) and $[Co_3(OH)_2(bdt)_2(bpp)_2(H_2O)_2]_n$ (**2**), which were synthesized by hydrothermal reaction from the respective tetrazole ligand (5-(4-pyridyl)tetrazole (4-H-ptz) for **1** and 5,5′-(1,4-phenylene)bis(1-*H*-tetrazole) (H_2bdt) for **2**), long and flexible pyridyl-containing ligand 1,3-bi(4-pyridyl)propane (bpp), NaN_3, and $CoCl_2$. Both **1** and **2** consist of well-isolated one-dimensional cobalt(II) alternating chains further linked by the bpp and/or the tetrazole ligand, while their chain structures are totally different. The chains of **1** are formed by Co^{2+} ions bridged by single μ-EE-N_3 and triple (μ-EO-N_3)(μ-tetrazole)$_2$ alternately, whereas the Co^{2+} ions are bridged by μ_3–OH to form $Co_3(OH)_2$ chains in compound **2**. Magnetic measurements demonstrate that compound **1** contains an alternating antiferromagnetic (AF)/ferromagnetic (FM) ferrimagnetic chain, while compound **2** exhibits the coexistence of spin canting, slow magnetic dynamics, and finite-size effect, with alternating AF/AF/FM ferrimagnetic chains.

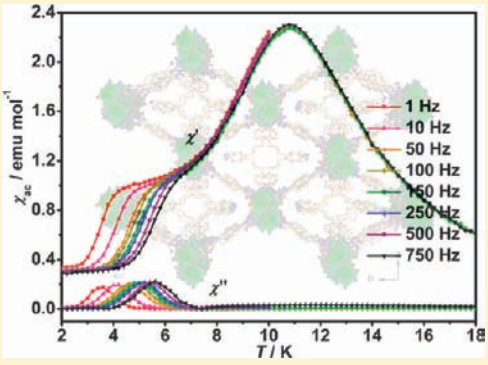

INTRODUCTION

Magnetic metal–organic frameworks have attracted a great deal of attention since they display fascinating structure and magnetic properties simultaneously.[1] They are helpful in understanding magneto-structural correlations and, therefore, provide an effective platform for further development of magnetic materials of academic and industrial interests. Different single-molecule magnets and single-chain magnets in short-range ordered ground states, ferromagnet, ferrimagnet, antiferromagnet, canted-antiferromagnet, and unusual meta-magnet in long-range ordered states have been synthesized and characterized.[1a,2] Despite the considerable success in this field, it still remains a major challenge to control and design the structure and structure–property relationship. Usually, to obtain a magnetic metal–organic framework, collecting paramagnetic transition-metal ions (Mn^{2+}, Fe^{2+}, Co^{2+}, Ni^{2+}, Cu^{2+}, et.al) with appropriate bridging ligands through a bottom-up approach is a general strategy. The bridging ligands always play a critical role. Carboxylate,[3] oxalate/oxamate,[4] cyano,[5] and azide[6] have been very widely used because of their ability to transmit magnetic coupling efficiently, but in recent years, there has been growing interest in nitrogen-containing heterocyclic ligands (pyrazole, imidazole, triazole, and tetrazole) due to their strong σ-electron donors to metals and diverse coordination modes, as well as their potential to construct molecular magnets.[7−9]

Here, we chose Co^{2+} ion as the paramagnetic center because the large single-ion magnetic anisotropy of it could lead to attractive magnetic characters, such as spin canting and slow magnetic relaxation.[2,10] As for the main organic ligands, we selected two 5-subsitituted 1H-tetrazoles derivatives, 5-(4-pyridyl)tetrazole (4-H-ptz) and 5,5-(1,4-phenylene)bis(1 H-tetrazole) (H_2bdt), due to their diverse coordination modes to afford various frameworks and their superexchange capacity reflected in interesting magnetic properties.[9a,11,12] However, in consideration of the rigidity of these two ligands and their difficulty in rotating, we also selected a flexible pyridyl-containing ligand, 1,3-bi(4-pyridyl)propane (bpp), and a small azide molecule as assistant ligands. Additionally, the long and nonconjugated bpp molecule could act as a diamagnetic separator, whereas the azide molecule could serve as an effective magnetic coupler with various bridging modes. In this Article, we report the synthesis, crystal structure, and magnetic properties of two metal–organic frameworks, $[Co_2(4\text{-ptz})_2(bpp)(N_3)_2]_n$ (**1**) and $[Co_3(OH)_2(bdt)_2(bpp)_2(H_2O)_2]_n$ (**2**). Both **1** and **2** display three-dimensional (3D) structure consisting of one-dimensional (1D) cobalt(II) alternating chains and interesting magnetic properties. In compound **1**, the Co^{2+} ion chains with alternating single μ-

Received: March 14, 2012
Published: June 1, 2012

   dx.doi.org/10.1021/ic300546z | *Inorg. Chem.* 2012, 51, 6813–6820

EE-N_3 and triple (μ-EO-N_3)(μ-tetrazole)$_2$ bridges are connected by the bpp and 4-ptz ligands to form a 3D structure. This structure exhibits intrachain alternating antiferromagnetic (AF)/ferromagnetic (FM) coupling. Compound **2** contains $Co_3(OH)_2$ chains bridged by μ_3−OH, extending to a 3D network through the bdt ligands. The magnetic properties of **2** indicate the coexistence of intrachain AF/AF/FM interaction, spin canting, slow magnetic relaxation, and finite-size effects.

EXPERIMENTAL SECTION

Synthesis. All reagents and solvents were commercially available and were used without further purification. 4-H-ptz and H_2bdt were synthesized according to literature methods.[13]

Preparation of $[Co_2(4\text{-ptz})_2(bpp)(N_3)_2]_n$ (1). $CoCl_2\cdot 6H_2O$ (0.0476 g, 0.2 mmol), 4-H-ptz (0.015 g, 0.1 mmol), bpp (0.02 g, 0.1 mmol), NaN_3 (0.033 g, 0.5 mmol), and distilled water (5 mL) were stirred briefly before the mixture was placed in a Teflon-lined stainless steel container and heated at 160 °C for 3 days under autogenous pressure. After cooling to room temperature, red block single crystals of **1** were recovered in a 45% yield based on 4-H-ptz. Anal. Calcd for $C_{25}H_{22}N_{18}Co_2$: C, 43.36; H, 3.20; N, 36.42. Found: C, 43.38; H, 3.22; N, 36.44. IR bands (cm^{-1}): 2920 w, 2858 w, 2098 s, 2064 s, 1620 s, 1561 m, 1450 m, 1223 m, 1010 m, 856 m, 802 m, 710 s, 530 m.

Preparation of $[Co_3(OH)_2(bdt)_2(bpp)_2(H_2O)_2]_n$ (2). $CoCl_2\cdot 6H_2O$ (0.0476 g, 0.2 mmol), H_2bdt (0.011 g, 0.05 mmol), bpp (0.02 g, 0.1 mmol), NaN_3 (0.033 g, 0.5 mmol), and distilled water (5 mL) were stirred briefly before the mixture was placed in a Teflon-lined stainless steel container and heated at 180 °C for 2 days under autogenous pressure. After cooling to room temperature, orange block single crystals of **2** were recovered in a 60% yield based on H_2bdt. Anal. Calcd for $C_{42}H_{42}N_{20}O_4Co_3$: C, 47.24; H, 3.96; N, 26.24. Found: C, 47.28; H, 3.88; N, 26.30. IR bands (cm^{-1}): 3548 m, 3083 m, 2936 m, 2850 w, 1609 s, 1550 m, 1506 w, 1430 s, 1230 m, 1007 m, 860 m, 800 m, 748 s, 500 m.

Caution: *Although not encountered in our experiments, azido compounds of metal ions are potentially explosive. Only a small amount of the materials should be prepared, and it should be handled with care.*

General Characterization. Elemental analyses of C, H, and N were carried out on a Perkin-Elmer 240C elemental analyzer. IR spectra as KBr pellets were recorded using a reflectance technique over the range of 4000−400 cm^{-1} on a Magna 750 FT-IR spectrophotometer (see Supporting Information, Figure S2). X-ray powder diffraction (XRPD) data were recorded at room temperature on a Rigaku D/max 2550 X-ray Powder Diffractometer. Thermogravimetric analysis (TGA) was carried out with a Metter-Toledo TA 50 in dry nitrogen (60 mL min^{-1}) in the temperature range of 20−900 °C (heating rate = 10°/min) (see Supporting Information, Figure S3). The TGA studies showed that compound **1** was stable up to near 320 °C and then began to decompose, and compound **2** began to decompose at about 200 °C.

Magnetic Measurements. The magnetic measurements of the compounds were carried out by use of Quantum Design SQUID MPMS-VSM magnetometer in the temperature range of 2−300 K and fields up to 5 T. Samples were fixed in gelatin capsules and held in a brass sample holder. Several temperature and field protocols were employed and will be described in the appropriate result section. Alternating current magnetic susceptibility measurements were performed in an oscillating ac field of 3.0 Oe, a 0, 200, and 1000 Oe Dc field. The oscillation frequencies were in the 1−850 Hz range. Pascal's constants were used to estimate the diamagnetic corrections, which were subtracted from the experimental susceptibilities to give the molar paramagnetic susceptibilities (χ_M).

X-ray Crystallography. Diffraction intensity data for the single crystal of the two compounds were carried out on Rigaku RAXIS-RAPID diffractometer equipped with a narrow-focus, 5.4 kW sealed tube X-ray source (graphite-monochromated Mo Kα radiation, λ = 0.710 73 Å) at 293 K. The data processing was accomplished with the PROCESS-AUTO processing program. The structures of the two compounds were solved by direct methods and refined with the full-matrix least-squares technique using the program SHELXTL.[14] All nonhydrogen atoms were easily found from the difference Fourier map. All hydrogen atoms of the organic molecule were placed by geometrical considerations and were added to the structure factor calculation. All nonhydrogen atoms were refined anisotropically. The crystal data, data collection, and refinement parameters for compounds **1** and **2** are listed in Table 1.

Table 1. Crystal Data and Structure Determination Summary for 1 and 2

	1	2
molecular formula	$C_{25}H_{22}N_{18}Co_2$	$C_{42}H_{42}N_{20}O_4Co_3$
formula weight	692.47	1067.75
temperature	293(2) K	293(2) K
wavelength	0.71073 Å	0.71073 Å
crystal system	orthorhombic	monoclinic
space group	*Pbcn*	*C*2/*c*
a/Å	15.230(3)	15.884(3)
b/Å	16.405(3)	22.496(5)
c/Å	13.939(3)	13.204(3)
β/deg		92.11(3)
V/Å^3	3482.7(12)	4715.0(16)
Z	4	4
D_{calc}, g/cm^3	1.321	1.504
μ	0.996 mm^{-1}	1.108 mm^{-1}
F(000)	1408	2188
GOF on F^2	1.034	1.042
final *R* indices $[I > 2\sigma(I)]^{a,b}$	R_1 = 0.0351	R_1 = 0.0789
	wR_2 = 0.0820	wR_2 = 0.1968
R indices (all data)	R_1 = 0.0489	R_1 = 0.1098
	wR_2 = 0.0881	wR_2 = 0.2173

$^aR_1 = \||F_o| - |F_c|\|/\sum|F|_o$. $^bwR_2 = [\sum w(F_o^2 - F_c^2)^2/\sum w(F_o^2)^2]^{1/2}$. $w = 1/[\sigma^2(F_o^2) + (ap)^2 + (bp)]$, $p = [\max(F_o^2, 0) + 2(F_c^2)]/3$.

RESULTS AND DISCUSSION

Synthesis and IR. The two compounds, $[Co_2(4\text{-ptz})_2(bpp)(N_3)_2]_n$ (**1**) and $[Co_3(OH)_2(bdt)_2(bpp)_2(H_2O)_2]_n$ (**2**), were obtained by the hydrothermal reaction at 160 and 180 °C of $CoCl_2$, 4-H-ptz/H_2bdt, bpp, and NaN_3 in a 2:1:1:5 and 4:1:2:10 molar ratio, respectively. Interestingly, azide does not participate in the construction of the framework of compound **2** but acts as a base to deprotonate the tetrazole ligand. We could not obtain any crystal when we did not use azide or used NaOH instead. The purity of both compounds was confirmed from their powder XRPD diffraction patterns which matched well with the calculated patterns obtained from their single crystal X-ray structures (Supporting Information, Figure S1).

The IR spectra of compound **1** (see the Experimental Section and Supporting Information, Figure S2) contain characteristic bands of the azido bridges and the tetrazole group. In the region expected for the ν_{as}-(N_3) absorption, the compound exhibits two strong bands at ca. 2098 and 2064 cm^{-1}, attributable to the presence of both μ-EE-N_3 and μ-EO-N_3 bridges in the structure.[15] The main IR characteristic peaks of compound **2** at ca.3548, 3083, and 1609 cm^{-1} can be attributed to hydroxyl group, coordinated water molecule, and tetrazole group, respectively.

Crystal Structures. *Structure of 1.* Single-crystal X-ray diffraction analysis reveals that **1** shows a 3D network

dx.doi.org/10.1021/ic300546z | Inorg. Chem. 2012, 51, 6813−6820

consisting of well-isolated 1D alternating Co(II) chains further linked by the 4-ptz and bpp ligands. Compound **1** crystallized in the orthorhombic space group *Pbcn*. The asymmetric unit consists of one Co^{2+} ion, one ptz^{-1} anion, one-half bpp ligand, and one azide anion. The Co atom assumes an octahedral coordination geometry completed by two tetrazole nitrogen atoms (N2 and N3A, Co−N = 2.1134(17) and 2.1984(17) Å) from two different 4-ptz, one pyridyl nitrogen atom from a 4-ptz ligand (N5A, Co−N = 2.1186(17) Å), one pyridyl nitrogen atom from a bpp ligand (N6, Co−N = 2.1430(19) Å), and another two nitrogen atoms (N7 and N9, Co−N = 2.102(2) and 2.1568(16) Å) from a EE-N_3 and a EO-N_3(Supporting Information, Figure S4). In the structure, two adjacent Co^{2+} ions connect each other through triple (μ-EO-N_3)(μ-tetrazole)$_2$ bridges into a dimeric unit, with the distance Co1A-Co1B = 3.495 Å. These dimeric units extend through a single μ-EE-N_3 to form a 1D chain along the *c* axis (Figure 1a). Therefore, the chain could be considered as an alternating chain with μ-EE-N_3 and (μ-EO-N_3)(μ-tetrazole)$_2$ bridges arranged alternately. This chain structure somewhat resembles that observed in another Co^{2+} compound reported by Gao et.al.,[16] where the chains are connected by coordinated Co^{2+} ion building blocks, resulting in a two-dimensional (2D) layer. In compound **1**, the 1D Co(II) chains extend to a 2D layer parallel to the *ac* plane through the bpp ligand (Figure 1b). Finally, each dimeric unit connects another four in a neighboring layer, forming a 3D net framework as shown in Figure 1c. The shortest Co−Co interchain distance is 9.616 Å. If we consider the dimeric unit as a node and the EE-N_3, 4-ptz, and bpp ligands as linkers, according to the analysis of Topos 4.0, the structure of **1** can be described as a 3D **ecu** network with the point (Schlafli) symbol ($3^6 \cdot 4^{15} \cdot 5^7$).

Structure of 2. Compound **2** is also a 3D framework based on 1D chains, but the chain structure is completely different from that of **1**. Compound **2** crystallized in the monoclinic space group *C*2/*c*. There are two categories of Co^{2+} ions (Co1 and Co2) in different coordination environments, and they both adopt distorted octahedral geometry (Supporting Information, Figure S5). Co1 is coordinated by two hydroxyl oxygen atoms (O1 and O1A, Co−O = 2.137(5) and 2.114(4) Å), two nitrogen atoms from two different bdt (N2 and N6A, Co−N = 2.146(5) and 2.149(5) Å), one pyridyl nitrogen atom from the bpp ligand (N9, Co−N = 2.181(6) Å), and one oxygen atom from a coordinated water molecule (O2, Co−O = 2.098(4) Å). Co2 is coordinated by four nitrogen atoms from four different bdt ligands (N3, N3A, N7A, N7B, Co−N = 2.132(5) and 2.126(5) Å) and two μ_3−OH group oxygen atoms (O1 and O1B, Co−O = 2.119(4) Å). The Co−O and Co−N bond distances are all within the normal ranges.[17] In the structure, Co^{2+} ions are bridged by μ_3−OH groups to form a $Co_3(OH)_2$ chain (Figure 2a), where three adjacent Co^{2+} ions are arranged into a triangle. Each triangle consists of a symmetrically related pair Co1 and Co1A and one Co2 atom. The Co1−Co1A = 3.147 Å, Co1A−Co2 = 3.935 Å, Co2−Co1 = 3.397 Å, respectively, and the Co1−O−Co1A, Co1A−O−Co2, and Co2−O−Co1 angles are 95.50(16), 136.8(2), and 105.93(19)°, respectively. As observed and confirmed in the cobalt hydroxyl derivatives,[18,19] the Co1 atoms sharing two μ_3−OH groups are related by ferromagnetic interaction, while antiferromagnetic coupling occurs between Co1 and Co2 and Co1A and Co2. To simplify, we neglect the antiferromagnetic interaction between Co1A and Co2, since the interaction may be much weaker than that between Co1 and Co2 because of the long Co1A−Co2 distance and large Co1A−O−Co2 angle.[20] Consequently, the chain could be considered as an alternating AF/AF/FM chain approximately (see the Magnetic Properties of 2 section). Finally, each 1D $Co_3(OH)_2$ chain is connected to four neighbors through the bdt ligands coordinated to Co2, resulting in a 3D structure as shown in Figure 2b. The shortest Co−Co interchain distance is 11.238 Å. This 3D structure displays a 1D channel along the *c* axis if taking no account of the bpp molecule. One side of the bpp coordinates to Co1, while the other side does not coordinate to

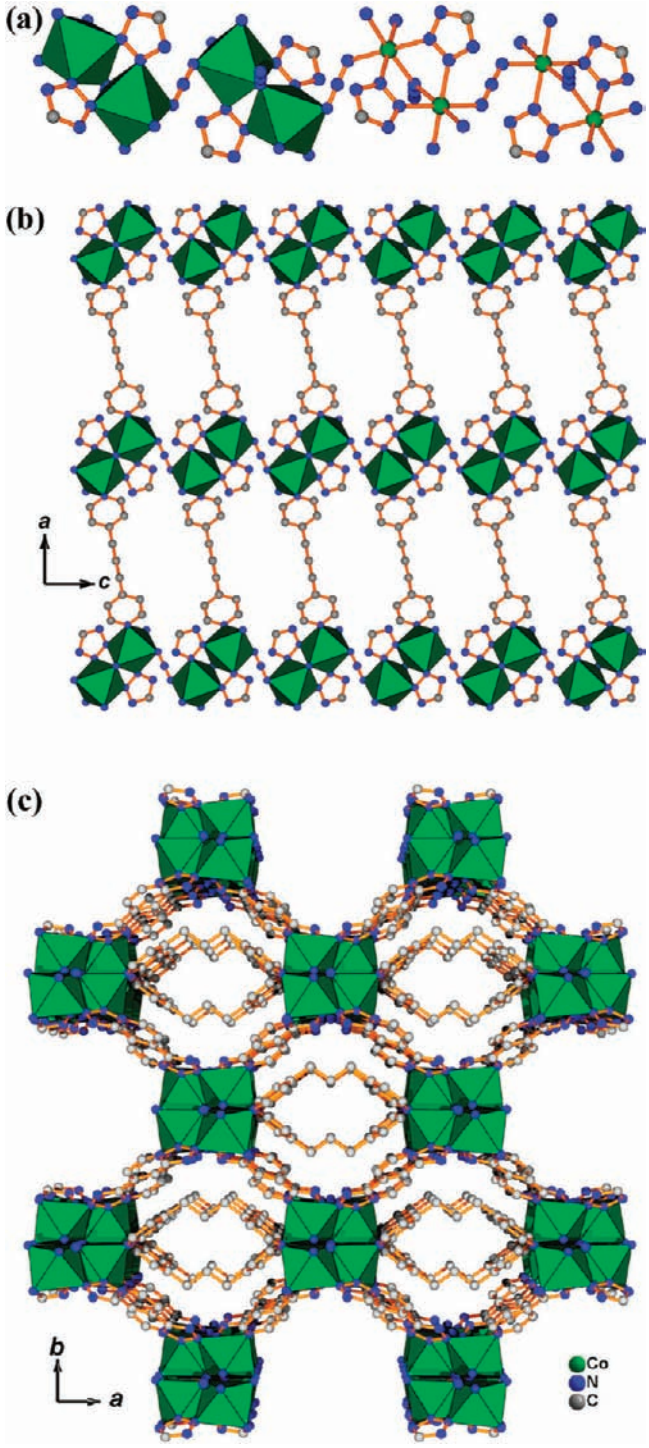

Figure 1. (a) View of the 1D chain, (b) 2D layer, and (c) 3D framework structure of **1**.

dx.doi.org/10.1021/ic300546z | *Inorg. Chem.* 2012, 51, 6813−6820

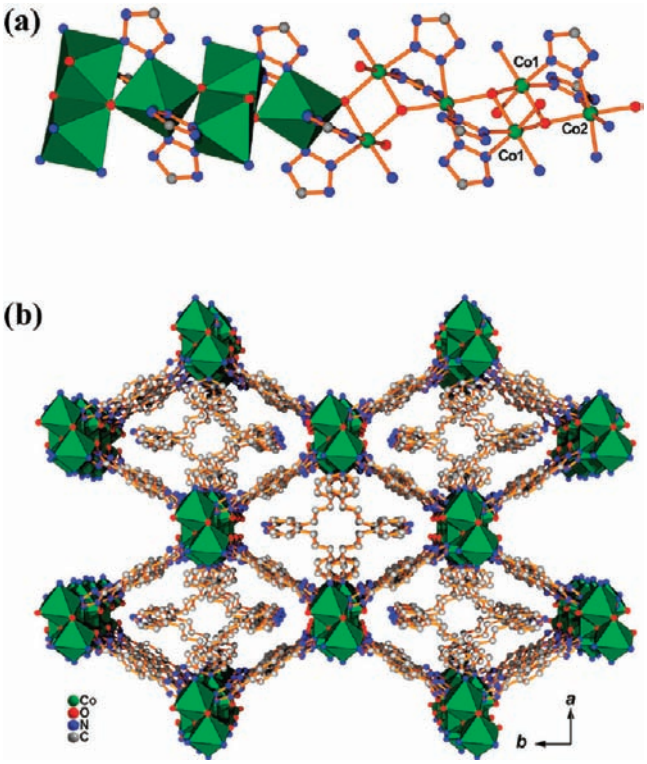

Figure 2. (a) View of the 1D chain and (b) 3D framework structure of **2**.

Co^{2+} ion but fills in the channel. If we consider Co2 as a node, the bdt ligand, and the dinuclear units formed by two Co1 as linkers, according to the analysis of Topos 4.0, the structure of **2** can be described as a 3D **pcu** network.

Magnetic Properties of 1. The magnetic susceptibility (χ) was measured on a crystalline sample with an applied field of 1000 Oe in the temperature range of 2−300 K. The magnetic properties of **1** in the form of χ_M versus T and $\chi_M T$ versus T per Co^{2+} ion are presented in Figure 3. At room temperature, the

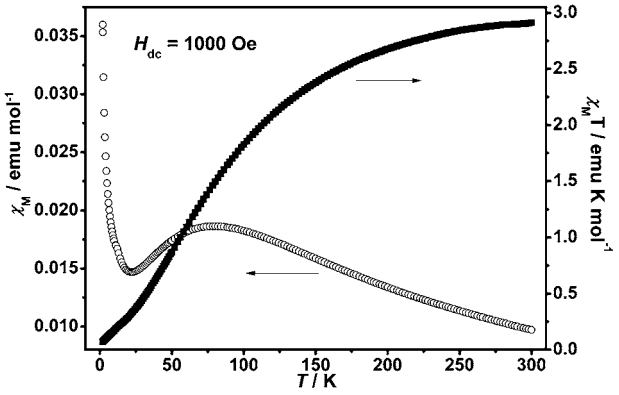

Figure 3. Magnetic susceptibility of **1** plotted as χ_M vs T and χ_MT vs T curves.

$\chi_M T$ value is 2.91 emu mol^{-1} K, larger than the spin only one expected for an isolated Co^{2+} ion (1.88 emu mol^{-1} K and S = 3/2), attributing to the significant orbital contribution of the Co^{2+} ion in the octahedral environment. Upon cooling, the $\chi_M T$ value decreases monotonically and reaches a minimum value of 0.07 emu mol^{-1} K at 2 K, but the temperature dependence of the susceptibility is more complex. As the temperature is lowered, the χ_M value keeps smoothly increasing and shows a rounded maximum of 0.019 emu mol^{-1} at about 80 K, then decreases to a minimum value of 0.015 emu mol^{-1} at 21 K, and finally increases rapidly to 0.036 emu mol^{-1} at 2 K.

According to the structural characteristics of **1**, there are two types of intrachain magnetic exchange pathways corresponding to different linkages, J_1 through the single μ-EE-N_3 bridge and J_2 through the mixed (μ-EO-N_3)(μ-tetrazole)$_2$ triple bridge. J_1 and J_2 are arranged alternately. To simulate the interaction in the chain roughly, we utilized an alternating 1D Heisenberg chain (S = 3/2) model ($H = -J_1\Sigma S_{2i}S_{2i+1} - J_2\Sigma S_{2i+1}S_{2i+2}$) incorporating λ as a correction item which takes care of both the orbital contribution due to the presence of spin−orbit coupling in the high-spin Co(II) system and the interchain antiferromagnetic interaction (Supporting Information).[21−23] The magnetic susceptibilities data above 35 K fit the model very well, giving the parameters J_1 = −31.2 cm^{-1}, J_2 = 40.2 cm^{-1}, g = 2.59, λ = −11.0 K, and $R = 7.9 \times 10^{-8}$, $R = [(\chi_M T)_{obsd} - (\chi_M T)_{calcd}]^2/[(\chi_M T)_{obsd}]^2$ (Supporting Information, Figure S6). The λ value is comparable with that observed in other Co(II) systems. The simulation indicates that the magnetic properties should be attributed to the competition between ferromagnetic interaction through the (μ-EO-N_3)(μ-tetrazole)$_2$ bridge and antiferromagnetic coupling through the μ-EE-N_3 bridge along the chain. Therefore, the chain could be considered as an alternating chain with AF-FM-AF-FM interaction. The result is consistent with that confirmed in the compound reported by Gao et.al.,[16] where the linkages between the Co^{2+} ions are similar to that of compound **1**. It is well established that μ-EE-N_3 prefers antiferromagnetic coupling, and it may not be surprising that the (μ-EO-N_3)(μ-tetrazole)$_2$ bridge transmits ferromagnetic interaction since there are still some other magnetic Co(II) systems with mixed (μ-EO-N_3)(μ-COO)$_2$, (μ-EO-N_3)$_2$(μ-COO), and (μ-EO-N_3)(μ-COO)(μ-tetrazole) bridges transmitting ferromagnetic interaction.[10a,24,26a]

The magnetic behavior in the low-temperature region deserves further investigation. Field-cooled (FC) magnetization measurements were performed under different fields (Supporting Information, Figure S7). On decreasing the temperature below 21 K, the χ_M value increases rapidly. Additionally, the field-cooled magnetization curve is independent of the applied field, which may preclude spin canting behavior. Therefore, the increase in χ_M at low temperature may be attributed to the residual spins resulting from the competition between ferromagnetic interaction through the (μ-EO-N_3)(μ-tetrazole)$_2$ bridge and antiferromagnetic coupling through the μ-EE-N_3 bridge along the chain. The field dependence of the magnetization for compound **1** at 2 K is shown in Supporting Information, Figure S8. The magnetization at 50 kOe reaches only 0.17 Nβ, which is much lower than the saturation value of Co^{2+}, verifying the presence of competition between ferromagnetic and antiferromagnetic coupling. Moreover, neither hysteresis loop nor peak of long-range magnetic ordering in Ac susceptibility data is observed for **1**.

Magnetic Properties of 2. The temperature dependence of the magnetic susceptibilities for **2** was measured at 1000 Oe in the temperature range of 2−300 K (Figure 4). The $\chi_M T$ value is 10.92 emu mol^{-1} K for a Co_3 unit, which is much larger than the spin only one expected for three isolated Co^{2+} ions (5.63 emu mol^{-1} K and S = 3/2) but falls within the usual range for octahedral Co^{2+} ion in the $^4T_{2\,g}$ state. As the temperature is

dx.doi.org/10.1021/ic300546z | Inorg. Chem. 2012, 51, 6813−6820

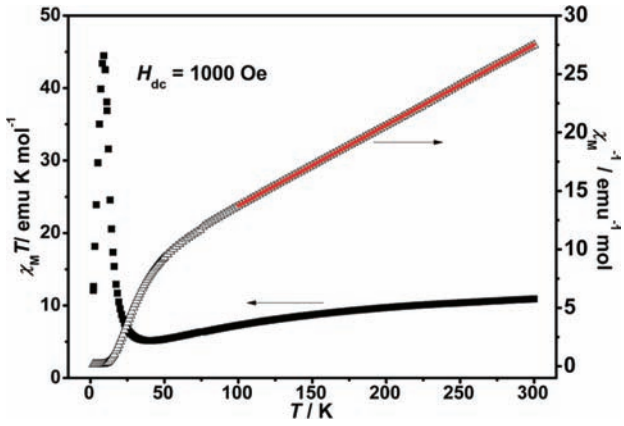

Figure 4. Magnetic susceptibility of **2** plotted as $\chi_M T$ vs T and $\chi_M{}^{-1}$ vs T curves.

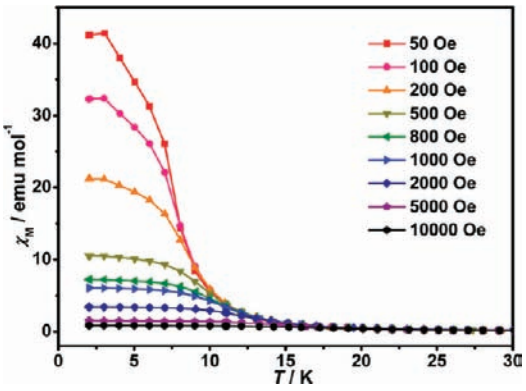

Figure 5. Temperature dependence of the field-cooled magnetic susceptibility of **2**.

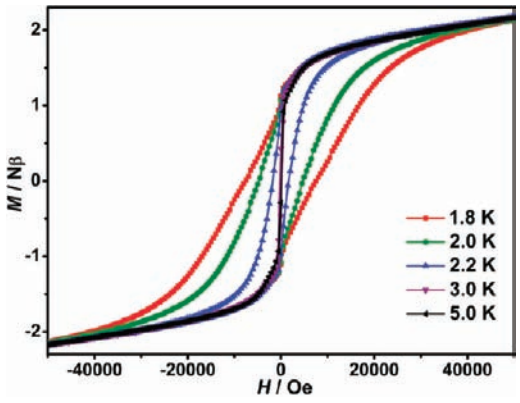

Figure 6. The isothermal field dependence of magnetization for **2**.

lowered, $\chi_M T$ first decreases gradually to a minimum of 5.16 emu mol^{-1} K at 41 K, then increases sharply to 44.47 emu mol^{-1} K at 9 K, and finally drops to 6.05 emu mol^{-1} K at 2 K rapidly. The phenomenon is reminiscent of ferrimagnetic behavior. The magnetic susceptibility above 75 K fits the Curie–Weiss law very well, giving C = 14.48 cm^3 mol^{-1} K and θ = −98.62 K. The C value corresponds to g = 3.21, and the large negative value of θ suggests a dominant antiferromagnetic coupling between Co^{2+} ions in the chain. It is noted that the depopulating of the higher Kramers doublets may also partially contribute to the large negative value of θ.[20]

Due to the complication of the large spin–orbit coupling of the Co^{2+} ions and the lack of an appropriate analytical expression for an anisotropic model of this complicated system, we chose an alternating 1D Heisenberg chain (S = 3/2) model ($H = -J_1\Sigma(S_{3i}S_{3i+1} + S_{3i+1}S_{3i+2}) - J_2\Sigma S_{3i-1}S_{3i}$, where J_1 is the intrachain coupling between Co1 and Co2 ions and J_2 is the intrachain coupling between Co1 ions) incorporating λ as a correction item.[25] The λ takes care of both the orbital contribution and the interchain antiferromagnetic interaction (Supporting Information). The magnetic susceptibility data above 40 K can be fitted well with J_1 = −24.6 cm^{-1}, J_2 = 6.2 cm^{-1}, g = 3.10, λ = −15.2 K, and $R = 6.1 \times 10^{-6}$, $R = [(\chi_M T)_{obsd} - (\chi_M T)_{calcd}]^2/[(\chi_M T)_{obsd}]^2$. (Supporting Information, Figure S9). The result is in agreement with our previous supposition about the AF/AF/FM ferrimagnetic chain (see the Structure of 2 section).

The zero-field-cooled magnetization (ZFC) and field-cooled magnetization (FC) data were measured at 50 Oe. The divergence below 5 K indicates the history dependence of the magnetization process (Supporting Information, Figure S10). Furthermore, the FC susceptibility data are rather field dependent, and the susceptibility decreases as the applied field increases (Figure 5), corresponding to canted antiferromagnetism. The spin canting may be caused by the antisymmetric exchange interaction between the Co^{2+} ions in the chain, as well as the single-ion magnetic anisotropy of Co^{2+}. Under low fields of 50, 100, and 200 Oe, the abrupt increase of χ_M below 10 K clearly exhibits the onset of spontaneous magnetization. At 1.8 K, the isothermal magnetization (Figure 6) displays an obvious hysteresis loop with a relatively large coercive field of 7650 Oe and remnant magnetization of 1.12 Nβ. The magnetization at 50 kOe is 2.14 Nβ, about 1/3 of the anticipated value for three ferromagnetic coupling Co^{2+} ions (S_{eff} = 1/2, <g> = 13/3), confirming the ferrimagneitic behavior again. On warming, the hysteresis loop diminishes drastically and almost disappears at 5 K, indicating that the material is a soft magnet.

As is shown in Figure 7, the Ac susceptibilities are temperature and frequency dependent under zero-applied Dc field, indicating slow magnetization dynamics. Interestingly, for the low frequency data (below 250 Hz), the in-phase component χ' displays a less frequency-dependent peak around 6.5 to 7.5 K and another rather frequency-dependent shoulder at lower temperature, and the out-of-phase component χ'' also displays a less frequency-dependent peak around 6 to 7 K and a rather frequency-dependent peak around 4 to 6 K. For higher frequency data (above 250 Hz), there is only one apparent peak in both χ' and χ'' data. We can conclude that the peak in higher temperature range for low frequency data is related to a second magnetic transition or finite-size effect because the peak of χ' shifts to higher temperature and the peak of χ'' is suppressed when a suitable Dc field is applied (see below). The shift of the peak temperatures T_p (the lower temperature ones for low frequency data below 250 Hz) of χ'' can be measured by the parameter $\phi = (\Delta T_p/T_p)/\Delta(\log f) = 0.21$, which is much larger than that for a canonical spin class, closer to the normal value for superparamagnets and single-chain magnets. The magnetic relaxation is fitted by the Arrhenius law, $\tau = \tau_0 \exp(\Delta_\tau/T)$, resulting in Δ_τ = 70 K and $\tau_0 = 5.1 \times 10^{-9}$ s, as shown in Supporting Information, Figure S13a. The Cole–Cole diagram at fixed temperature around the cusp of χ'' is shown in Supporting Information, Figure S11, and the data at 5.6 K can be well fitted by a generalized Debye model with an α = 0.29, which lies in the normal range of single-chain magnets (SCM).

dx.doi.org/10.1021/ic300546z | Inorg. Chem. 2012, 51, 6813–6820

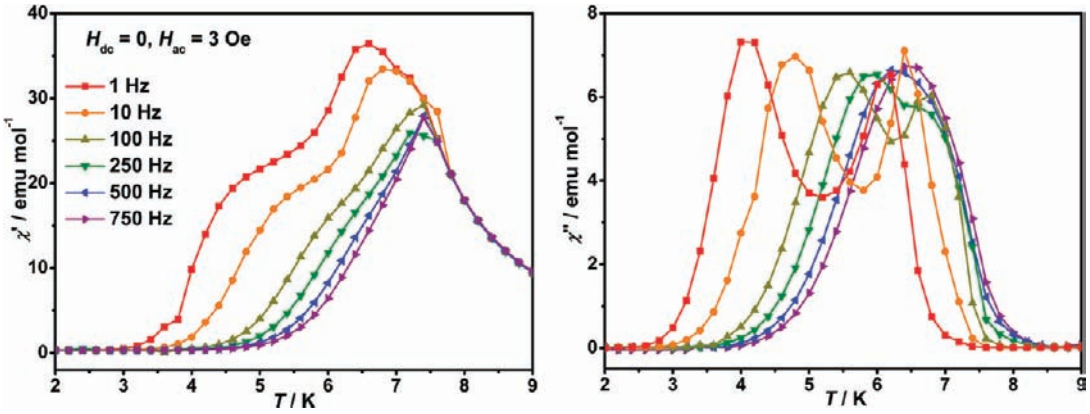

Figure 7. The ac magnetic susceptibility of **2** at different frequencies with a driving ac field of 3 Oe under zero static field.

The zero field Ac magnetic susceptibility data are also shown in $\ln(\chi'T)$ versus $1/T$ form in Figure 8. The maximum around

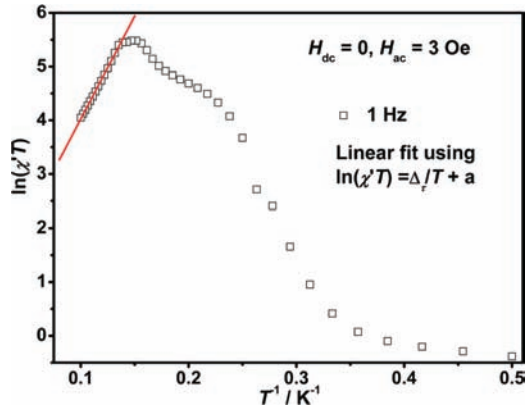

Figure 8. Semilogarithmic plot of $\chi'T$ vs $1/T$. The data were obtained from ac measurements at 3 Oe and 1 Hz at zero dc field.

6.8 K may be indicative of finite-size effects ($\xi \gg L$).[26] A linear variation of $\ln(\chi'T)$ vs $1/T$ is also observed, where the corresponding slope gives the creation energy for a domain wall along the chain, Δ_ξ = 39 K. For a finite chain, the expression of Δ_τ is: $\Delta_\tau = \Delta_A + \Delta_\xi$. Therefore, the antisotropic barrier for the reversing of the magnetization of an individual magnetic unit can be obtained as $\Delta_A = 70 - 39 = 31$ K.

To gain more insight into the dynamic characteristics, we measured the Ac susceptibilities in 200 and 1000 Oe applied Dc fields (Figures 9 and 10). Under 200 Oe Dc field, χ' of all the frequencies exhibits a frequency-independent maximum at 8.2 K and a frequency-dependent shoulder around 4 to 6 K. χ'' shows only one frequency-dependent peak in the temperature range of 3 to 6 K. The peak around 6 to 7 K for the low frequency data below 250 Hz seems to be partly suppressed. The shift of the peak temperature T_p of χ'' measured by the parameter $\phi = (\Delta T_p/T_p)/\Delta(\log f) = 0.20$ and the relaxation time follow the Arrhenius law with $\Delta\tau$ = 68 K and $\tau_0 = 3.3 \times 10^{-9}$ s (Supporting Information, Figure S13b). Under 1000 Oe static field, the frequency-independent peak of χ' shifts to 10.8 K and the frequency-dependent shoulder becomes more pronounced. The cusp of χ'' is a little shifted to lower temperature, and the peaks around 6 to 7 K observed under zero Dc field for the low frequency data are completely suppressed. Figure S13c (Supporting Information) shows the Arrhenius law with Δ_τ = 67 K and $\tau_0 = 1.5 \times 10^{-9}$ s, and Figure S12 (Supporting Information) displays the Cole−Cole curves around 4.2 to 6.2 K. The fit to the generalized Debye model at 5.4 K gives the parameter α = 0.13. These phenomena confirm the SCM behavior with finite size effect in compound **2**.

CONCLUSIONS

In summary, we reported the synthesis, structures, and magnetic properties of two three-dimensional metal−organic frameworks with 5-subsitituted 1H-tetrazoles derivatives as main ligands. Both compounds contain one-dimensional cobalt(II) alternating chains further linked by the bpp and/or tetrazole ligands, but their chain structures are completely different. For **1**, the Co^{2+} ions are alternately bridged by a single

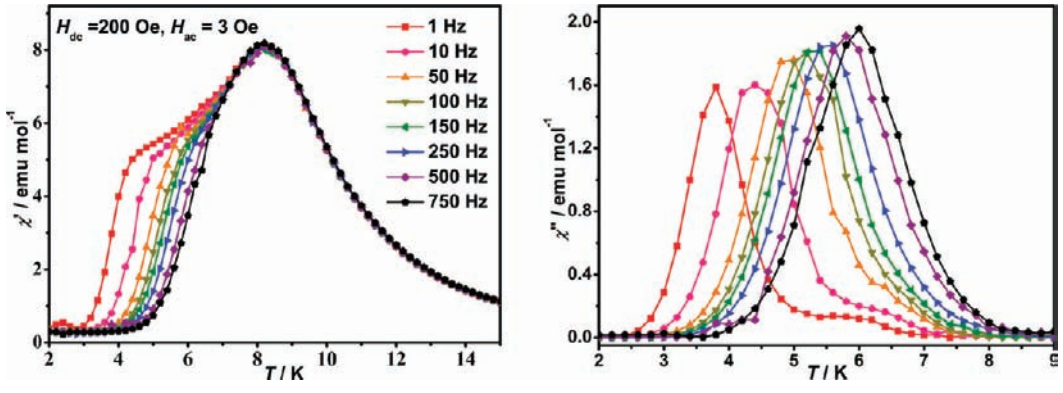

Figure 9. The ac magnetic susceptibility of **2** at different frequencies with a driving ac field of 3 Oe under 200 Oe static field.

dx.doi.org/10.1021/ic300546z | Inorg. Chem. 2012, 51, 6813−6820

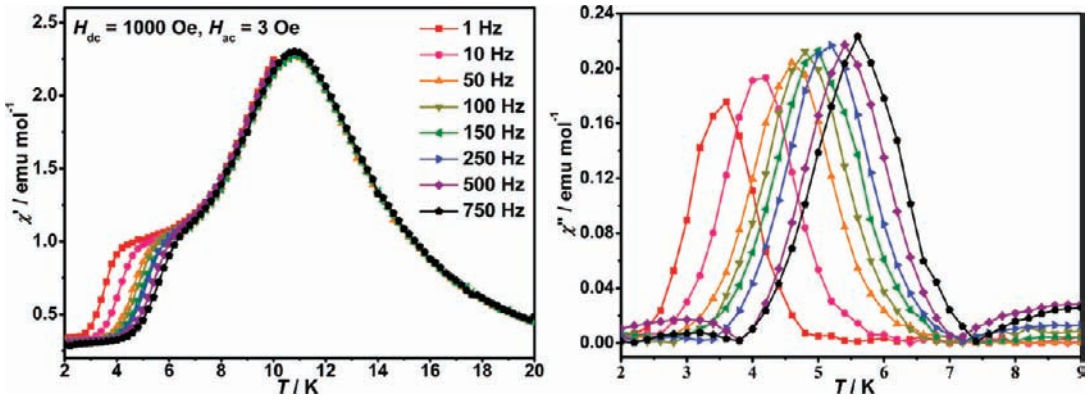

Figure 10. The ac magnetic susceptibility of **2** at different frequencies with a driving ac field of 3 Oe under 1000 Oe static field.

μ-EE-azide and a triple (μ-EO-azide)(μ-tetrazole)$_2$ bridge in the chain, and the Co^{2+} ions are mixed bridged by μ_3−OH groups to form $Co_3(OH)_2$ chain in **2**. Magnetic measurements demonstrate that the chains of both compounds show ferrimagnetic behavior. Additionally, compound **2** exhibits the coexistence of spin canting, slow magnetic dynamics, and finite-size effect.

■ ASSOCIATED CONTENT

Supporting Information

X-ray crystallographic data of **1** and **2** in CIF format, powder XRD patterns data, and some magnetic plots. This material is available free of charge via the Internet at http://pubs.acs.org.

■ AUTHOR INFORMATION

Corresponding Author

*E-mail: zshi@mail.jlu.edu.cn. Phone: +86-431-85168662. Fax: +86-431-85168624.

Notes

The authors declare no competing financial interest.

■ ACKNOWLEDGMENTS

This work was supported by the Foundation of the National Natural Science Foundation of China (No. 20971054 and 90922034) and Specialized Research Fund for the Doctoral Program of Higher Education

■ REFERENCES

(1) (a) Kurmoo, M. *Chem. Soc. Rev.* **2009**, *38*, 1353. (b) Rowsell, J. L. C.; Yaghi, O. M. *Microporous Mesoporous Mater.* **2004**, *73*, 3. (c) Ohtani, R.; Yoneda, K.; Furukawa, S.; Horike, N.; Kitagawa, S.; Gaspar, A. B.; Muñoz, M. C.; Real, J. A.; Ohba, M. *J. Am. Chem. Soc.* **2011**, *133*, 8600. (d) Pardo, E.; Train, C.; Gontard, G.; Boubekeur, K.; Fabelo, O.; Liu, H. B.; Dkhil, B.; Lloret, F.; Nakagawa, K.; Tokoro, H.; Ohkoshi, S. I.; Verdaguer, M. *J. Am. Chem. Soc.* **2011**, *133*, 15328.

(2) (a) Sun, Q.; Cheng, A. L.; Wang, Y. Q.; Ma, Y.; Gao, E. Q. *Inorg. Chem.* **2011**, *50*, 8144. (b) Zhao, J. P.; Hu, B. W.; Zhang, X. F.; Yang, Q.; Fallah, M. S. E.; Bu, X. H. *Inorg. Chem.* **2010**, *49*, 11325.

(3) (a) Zhao, J. P.; Hu, B. W.; Lloret, F.; Tao, J.; Yang, Q.; Zhang, X. F.; Bu, X. H. *Inorg. Chem.* **2010**, *49*, 10390. (b) Li, Z. X.; Zhao, J. P.; Saňudo, E. C.; Ma, H.; Pan, Z. D.; Zeng, Y. F.; Bu, X. H. *Inorg. Chem.* **2009**, *48*, 11601. (c) Zheng, Y. Z.; Tong, M. L.; Zhang, W. X.; Chen, X. M. *Angew. Chem., Int. Ed.* **2006**, *45*, 6310.

(4) (a) Coronado, E.; Mascarós, J. R. G.; Gastaldo, C. M. *J. Am. Chem. Soc.* **2008**, *130*, 14987. (b) Pardo, E.; Garcia, R. R.; Lloret, F.; Faus, J.; Julve, M.; Journaux, Y.; Novak, M. A.; Delgado, F. S.; Perez, C. R. *Chem.—Eur. J.* **2007**, *13*, 2054.

(5) Toma, L. M.; Lescouezec, R.; Pasan, J.; Perez, C. R.; Vaissermann, J.; Cano, J.; Carrasco, R.; Wernsdorfer, W.; Lloret, F.; Julve, M. *J. Am. Chem. Soc.* **2006**, *128*, 4842.

(6) (a) Liu, T. F.; Fu, D.; Gao, S.; Zhang, Y. Z.; Sun, H. L.; Su, G.; Liu, Y. J. *J. Am. Chem. Soc.* **2003**, *125*, 13976. (b) Sun, H. L.; Wang, Z. M.; Gao, S. *Chem.—Eur. J.* **2009**, *15*, 1757.

(7) (a) Banerjee, R.; Phan, A.; Wang, B.; Knobler, C.; Furukawa, H.; O'Keeffe, M.; Yaghi, O. M. *Science* **2008**, *319*, 939. (b) Wang, B.; Côté, A. P.; Furukawa, H.; O'Keeffe, M.; Yaghi, O. M. *Nature* **2008**, *453*, 207.

(8) Zhao, H.; Qu, Z. R.; Ye, H. Y.; Xiong, R. G. *Chem. Soc. Rev.* **2008**, *37*, 84−100.

(9) (a) Ouellette, W.; Darling, K.; Prosvirin, A.; Whitenack, K.; Dunbar, K. R.; Zubieta, J. *Dalton Trans.* **2011**, *40*, 12288. (b) Sengupta, O.; Mukherjee, P. S. *Inorg. Chem.* **2010**, *49*, 8583.

(10) (a) Murrie, M. *Chem. Soc. Rev.* **2010**, *39*, 1986. (b) Wang, Y. Q.; Zhang, X. M.; Li, X. B.; Wang, B. W.; Gao, E. Q. *Inorg. Chem.* **2011**, *50*, 6314. (c) Zhang, X. M.; Jiang, T.; Wu, H. S.; Zeng, M. H. *Inorg. Chem.* **2009**, *48*, 4536.

(11) (a) Luo, T. T.; Tsai, H. L.; Yang, S. L; Liu, Y. H.; Yadav, R. D.; Su, C. C.; Ueng, C. H.; Lin, L. G.; Lu, K. L. *Angew. Chem., Int. Ed.* **2005**, *44*, 6063. (b) Ouellette, W.; Liu, H. X.; O'Connor, C. J.; Zubieta, J. *Inorg. Chem.* **2009**, *48*, 4655. (c) Dong, P.; Zhang, Q. K.; Wang, F.; Chen, S. C.; Wu, X. Y.; Zhao, Z. G.; Lu, C. Z. *Cryst. Growth Des.* **2010**, *10*, 3218.

(12) Ouellette, W.; Prosvirin, A. V.; Whitenack, K.; Dunbar, K. R.; Zubieta, J. *Angew. Chem., Int. Ed.* **2009**, *48*, 2140.

(13) (a) Demko, Z. P.; Sharpless, K. B. *J. Org. Chem.* **2001**, *66*, 7945. (b) Tao, J.; Ma, M. J.; Huang, R. B.; Zheng, L. S. *Inorg. Chem.* **2004**, *43*, 6133.

(14) Sheldrick, G. M. *SADABS, the Siemens Area Detector Absorption Correction*; University of Göttingen: Göttingen, Germany, 2005.

(15) Tandon, S. S.; Thompson, L. K.; Manuel, M. E.; Bridson, J. N. *Inorg. Chem.* **1994**, *33*, 5555.

(16) Li, R. Y.; Gao, S. *Chin. J. Inorg. Chem* **2008**, *24*, 1229.

(17) Gutschke, S. O. H.; Price, D. J.; Powell, A. K.; Wood, P. T. *Angew. Chem., Int. Ed.* **2001**, *40*, 1920.

(18) Zhang, X. M.; Hao, Z. M.; Zhang, W. X.; Chen, X. M. *Angew. Chem., Int. Ed.* **2007**, *46*, 3456.

(19) (a) Li, X. J.; Wang, X. Y.; Gao, S.; Cao, Y. *Inorg. Chem.* **2006**, *45*, 1508. (b) Livage, C.; Férey, G. *Chem. Mater.* **1999**, *11*, 1546. (c) Huang, Z. L.; Drillon, M.; Masciocchi, N.; Sironi, A.; Zhao, J. T.; Rabu, P.; Panissod, P. *Chem. Mater.* **2002**, *12*, 2805. (d) Kumagai, H.; Kepert, C. J.; Kurmoo, M. *Inorg. Chem.* **2002**, *41*, 3410.

(20) Angelov, S.; Drillon, M.; Zhecheva, E.; Stoyanova, R.; Belaiche, M.; Derory, A.; Herr, A. *Inorg. Chem.* **1992**, *31*, 1514.

(21) (a) Cortés, R.; Drillon, M.; Solans, X.; Lezama, L.; Rojo, T. *Inorg. Chem.* **1997**, *36*, 677. (b) Abu-Youssef, M. A. M.; Drillon, M.; Escuer, A.; Goher, M. A. S.; Mautner, F. A.; Vicente, R. *Inorg. Chem.* **2000**, *39*, 5022. (c) Cano, J.; Journaux, Y.; Goher, M. A. S.; Abu-

Youssef, M. A. M.; Mautner, F. A.; Rei*β*, G. J.; Escuer, A.; Vicente, R. *New J. Chem.* **2005**, *29*, 306.
(22) (a) Zhang, X. M.; Li, C. R.; Zhang, X. H.; Zhang, W. X.; Chen, X. M. *Chem. Mater.* **2008**, *20*, 2298. (b) Cheng, X. N.; Zhang, W. X.; Chen, X. M. *J. Am. Chem. Soc.* **2007**, *129*, 15738.
(23) Kumagaia, H.; Okab, Y.; Inouea, K.; Kurmoo, M. *J. Phys. Chem. Solids.* **2004**, *65*, 55.
(24) Li, X. B.; Zhang, J. Y.; Wang, Y. Q.; Song, Y.; GAo, E. Q. *Chem.—Eur. J.* **2011**, *17*, 13883.
(25) (a) Abu-Youssef, M. A. M.; Drillon, M.; Escuer, A.; Goher, M. A. S.; Mautner, F. A.; Vicente, R. *Inorg. Chem.* **2000**, *39*, 5022. (b) Palli, A. V.; Tsukerblat, B. S.; Klokishner, S.; Dunbar, K. R.; Clemente-Juan, J. M.; Coronado, E. *Chem. Soc. Rev.* **2011**, *40*, 3130. (c) Palii, A. V.; Reu, O. S.; Ostrovsky, S. M.; Klokishner, S. I.; Tsukerblat, B. S.; Sun, Z. M.; Mao, J. G.; Prosvirin, A. V.; Zhao, H. H.; Dunbar, K. R. *J. Am. Chem. Soc.* **2008**, *130*, 14729. (d) Palli, A. V.; Ostrovsky, S. M.; Klokishner, S. I.; Reu, O. S.; Sun, Z. M.; Prosvirin, A. V.; Zhao, H. H.; Mao, J. G.; Dunbar, K. R. *J. Phys. Chem. A* **2006**, *110*, 14003. (e) Palii, A. V.; Tsukerblat, B. S.; Coronado, E.; Clemente-Juan, J. M.; Borrás-Almenar, J. J. *Inorg. Chem.* **2003**, *42*, 2455.
(26) (a) Zhang, X. M.; Wang, Y. Q.; Wang, K.; Gao, E. Q.; Liu, C. M. *Chem. Commum.* **2011**, *47*, 1815. (b) Coulon, C.; Miyasaka, H.; Clérac, R. *Struct. Bonding (Berlin)* **2006**, *122*, 163. (c) Bogani, L.; Caneschi, A.; Fedi, M.; Gatteschi, D.; Massi, M.; Novak, M. A.; Pini, M. G.; Rettori, A.; Sessoli, R.; Vindigni, A. *Phys. Rev. Lett.* **2004**, *92*, 207204.